


Article

Efficient and Reliable Power-Conditioning Stage for Fuel Cell-Based High-Power Applications

Mehroze Iqbal ^{1,2}, Amel Benmouna ^{1,2,3}, Frederic Claude ⁴ and Mohamed Becherif ^{1,*}¹ FEMTO-ST Institute, University Bourgogne Franche-Comte, UTBM, CNRS, 90000 Belfort, France² Department of Electrical Engineering, Universiti Tenaga Nasional, 43009 Kajang, Selangor, Malaysia³ School of Business and Engineering, ESTA Belfort, 90000 Belfort, France⁴ Segula Matra Technologies, 25200 Montbeliard, France

* Correspondence: mohamed.becherif@utbm.fr

Abstract: Mainstream power-conditioning devices such as boost converters are frequently utilized for developing a compatible interface between a fuel cell, electrical storage, and high power loads. The conventional power stage comprising a unique boost converter suffers from low efficiency and poor reliability due to excessive power losses, particularly in high-power applications. Additionally, the presence of high ripple contents can reduce the lifespan of the fuel cell itself. With this background, this paper proposes and experimentally validates a physical components-assisted equivalent power-sharing strategy between parallel-coupled boost converters (PCCs) that is subjected to a wide spectrum of low-voltage–high-power conditions. The operation of PCCs is bottlenecked by several practical limitations, such as the presence of inner circulating currents (ICCs) and stability issues associated with the equivalent sharing of power. To overcome these limitations, a module of reverse blocking diodes is suggested to avoid ICCs between the PCCs. Further, an equalization filter is properly placed to improve the equivalent power-sharing capability. The proposed strategy is theoretically assessed in a MATLAB/Simulink environment with a 6 kW proton exchange membrane fuel cell (PEMFC) as the main power source. A scaled-down laboratory setup consisting of an 810 W PEMFC stack, an electronic load, three boost converters, and a filter circuit is then designed and critically evaluated. A consistent agreement is observed between the experimental findings and the simulation results under realistic operating conditions.

Keywords: fuel cell; power conditioning; boost converters; equalization filter; experimental setup



Citation: Iqbal, M.; Benmouna, A.; Claude, F.; Becherif, M. Efficient and Reliable Power-Conditioning Stage for Fuel Cell-Based High-Power Applications. *Energies* **2023**, *16*, 4915. <https://doi.org/10.3390/en16134915>

Academic Editors: Felix Barreras and Fangming Jiang

Received: 13 April 2023

Revised: 6 June 2023

Accepted: 15 June 2023

Published: 24 June 2023



Copyright: © 2023 by the authors. Licensee MDPI, Basel, Switzerland. This article is an open access article distributed under the terms and conditions of the Creative Commons Attribution (CC BY) license (<https://creativecommons.org/licenses/by/4.0/>).

1. Introduction

The notion of green energy and the realization of a low-carbon economy is encouraging the widespread application of various renewable energy sources, such as fuel cell (FC) technology, in a variety of high-power (HP) applications [1–4]. The transportation sector is a prime example; here, FC technology is gradually replacing conventional combustion engines [5,6]. Another example is the integration of electrolyzer setups for complementing the intermittency of renewable generation [4,7,8]. Essentially, these examples consist of a low-voltage (LV) power source coupled with HP load through one or more power-conditioning stages [9,10]. Modern power electronic devices, such as the boost converter (BC), are extensively utilized to implement such stages [11–13]. Efficiency and reliability are the two most important concerns here, especially in LV–HP applications [14,15]. Both of these concerns are related to power losses in various components of power converters, such as switching devices and passive elements [16]. These power losses can be significant enough to negatively influence the operating efficiency, produce thermal throttling, and negatively affect the lifespan of the components [16,17]. Likewise, the presence of high ripple components due to the use of a conventional boost converter (CBC) can significantly degrade the lifespan and performance of the FC itself [18,19].

To enhance the efficiency and reliability of the power-conditioning phase in FC-based HP applications, an appropriate distribution of processed power among parallel-coupled converters (PCCs) is a viable solution. A considerable reduction in power losses can be achieved alongside noticeable improvements in conditioning efficiency [17,20]. The equivalent sharing of conditioned power between PCCs can also reduce the thermal throttling of the components. Likewise, due to the inherent redundancy of PCCs, power can still be processed in the case of a fault or failure [21,22]. However, ensuring the equivalent and safe sharing of conditioned power in PCCs is a difficult task. The conversion stage of PCCs is prone to various practical problems, such as undesirable inner circulation currents (ICCs) between the converters and stability problems associated with the unequal sharing of conditioned power [23].

1.1. Literature Review

An FC generally exhibits soft electrical characteristics, meaning that the voltage varies nonlinearly according to the loading conditions [24,25]. Further, despite having a profound capability to deliver higher power, it is primarily an LV source [18]. To develop a compatible connection between an LV power source and an HP load, a dedicated power-conditioning stage is a prerequisite [26]. Given its importance, this issue is rigorously addressed in the literature. A unique BC-based power stage is proposed and experimentally validated in [25] to interface an FC with a dynamic load. Due to the nonminimum phase nature of the BC, a nonlinear adaptive backstepping controller is designed to accommodate the nonlinearity of the FC and the uncertainty of the load. Similarly, an adaptive nonlinear sliding mode control is proposed in [27] for the tight regulation of a DC-bus to a desired value. In [18], modelling of low-frequency ripples in the FC current profile is performed. These ripples are produced due to the switching behavior of the conventional power-conditioning unit. It is highlighted by the authors that the low-frequency current ripples produced by the conventional CBC can significantly degrade the performance, efficiency, reliability, and lifespan of the FC. Therefore, designing a power stage with low current ripples is of paramount importance for enhancing the lifespan of FCs.

A CBC generally has several bottlenecks, such as low voltage gain, high system stresses, and poor efficiency [24,28]. Cascading multiple converters in a series (for high voltage gain) or connecting them in parallel (for high power) is a convenient solution to address these problems. A general discussion on the different types of connections between DC–DC converters is presented in [29]. Further, several modularization schemes with decentralized controllers are tested under diverse operating conditions. In [30], bi-directional DC–DC converters are connected in parallel to interface an AC motor drive with an LV battery. To reduce the circulation losses in the PCCs, a feedforward current-fed control is established. A 4 kW prototype is built and tested for validating the strategy. An interleave BC (IBC) is proposed in [31] for a photovoltaic (PV) source under partial shading conditions for reducing the ripples and stresses from the system. However, only operation with a PV main source is explicitly considered. The proposed parallel power stage (PPS) is an alternative and not a direct competitor to the widely accepted and viable interleave power stage, and it aims to deliver similar advantages. The interleave stage does not require any additional hardware, which is potentially necessary for the stable and efficient operation of the proposed PPS. However, the interleave stage does require a complex control with a phase-delay mechanism as the parallel legs are operated out of phase with each other. Moreover, IBCs are usually built from ground up for a specific application or a range of applications, while several similar conventional converters can be coupled in parallel to develop PCCs, thus providing modularity and scalability.

A high-current gain step-down resonant converter is suggested in [15] for HP applications, considering an ideal DC source. A large signal criterion-based control is proposed in [32] for PV and/or battery storage coupled with PCCs. With an FC as the main power source, an IBC is utilized in [28] for interfacing the FC with a DC-bus. Similarly, a wide-range interleaved converter is utilized in [24] for FC-based traction applications. A

high-conversion ratio non-isolated IBC is designed in [26] for FC-based applications. A parallel topology is utilized to minimize the ripples in the FC current. Similarly, a compact interleaved converter is developed in [33] for FC-based traction applications to increase the power density of the conversion stage and to reduce the current ripples.

To address the problems associated with PCCs, the following solution strategies have been proposed: (i) centralized control strategies to endorse balanced power sharing and a reduction in ICCs [20,34]; (ii) decentralized strategies consisting of droop controllers that do not require a central communication block [23,35]; and (iii) physical components-assisted methodologies to stabilize equivalent power sharing and improve efficiency [11,36]. To integrate various DC sources with the AC grid, an architecture composed of PCCs is proposed in [35]. A decentralized controller with a V–I droop scheme and without the need for a central communication block is considered. A decentralized controller based on an I–V droop scheme is developed in [22] for eliminating the problems associated with parallel-coupled DC–DC converters in HP applications. The controller is compared with a V–I droop scheme, and the authors illustrate that I–V droop controllers provide a comparatively faster transient response. Likewise, a decentralized control strategy is proposed in [21] for appropriate power sharing between parallel-connected bi-directional converters in grid-integration applications. A similar control strategy is adopted in [15] for equivalent power sharing between parallel-coupled resonant converters. Rather than a decentralized droop scheme, a master–slave controller is suggested in [34] to handle efficient power distribution between the PCCs. The authors of [34] conclude that for master–slave control, intercommunication between the converters is required to enable it to provide better performance than a decentralized controller, though at the cost of several communication blocks and a more complicated structure. Most of the strategies discussed here are based on flexible control/communication. Nevertheless, dedicated physical components are also proposed in the literature. An IBC is developed and preferred over PCCs in [31] for reducing the harmonics and current ripples in PV-based HP applications. An experimental setup consisting of PCCs and a passive equalization filter (PEF) is employed in [36] to study the behavior of PCCs under diverse operating conditions.

1.2. Highlighted Contributions

This paper contributes a physical components-assisted power-sharing strategy between parallel-coupled BCs. The proposed power-conversion stage is especially suitable for FC-interfaced LV–HP applications. A comprehensive comparison between the CBC and the proposed PCCs was performed to determine their relative efficiency and reliability in diverse operating conditions. The data presented in Table 1 lay the foundations of this comparison.

Table 1. Qualitative comparison between the studied power-conditioning stages.

Attributes	Conventional Boost Converter (CBC)	Parallel-Coupled Boost Converters (PCCs)
Efficiency	Poor due to higher losses	Enhanced due to power sharing
Reliability	No backup in case of failure	Redundancy
Placement	Informal	Challenging in confined spaces
Protection	Not required	Required to protect against ICCs
Control design	Simple for regulation output	Sophisticated

In [28], an IBC is utilized to interface an FC with a DC-bus for electrical traction applications. The overall harmonics profile is lower, and this enhances the overall reliability. Likewise, in [26,33], compact and high-voltage gain IBCs are developed and tested under various HP scenarios. The proposed power stages reduced the low frequency ripples from the FC current profile, thereby enhancing the lifespan of the components. However, an effective comparison between a CBC and an IBC power stage with respect to efficiency and reliability is not performed in any of these works. An experimental setup consisting of PCCs and a PEF is employed in [36] to study the behavior of PCCs under diverse operating

conditions. Here, a comprehensive comparison is performed between a CBC and PCCs. However, the behavior of an FC is emulated using a programmable supply, and the actual nonlinear characteristics of an FC are not considered. In [18], the negative effects of low-frequency ripples on FC reliability and efficiency are comprehensively studied. However, whether an appropriate solution composed of PCCs could reduce these ripples is not considered. Compared with the already existing studies, this paper makes the following contributions and improvements:

- An efficient and reliable module of PCCs is developed. The proposed module is specifically suitable for FC-based HP applications under a wide range of LV conditions.
- The practical shortcomings associated with PCCs, such as ICCs and stability issues related to equivalent power sharing, are properly addressed using hardware compensation.
- A dedicated structure of reverse blocking diodes (RBDs) is incorporated for suppressing the ICCs. In addition, an equalization filter (EF) is correctly placed to promote uniform power sharing between the interconnected converters.
- A graphical comparison is established to quantize the key performance indicators (efficiency and power losses) of the proposed PCCs under diverse HP conditions.
- The equivalent power-sharing capability and superior efficiency of the proposed PCCs is appraised by an experimental setup consisting of a proton exchange membrane FC (PEMFC), an electronic load, three converters coupled in parallel, and an EF circuit.

The rest of this paper is organized as follows: Section 2 details the system topology and the components used. The numerical simulations and a corresponding discussion are presented in Section 3. The particulars of the experimental setup along with the obtained results are given in Section 4. Finally, our conclusions and perspectives are presented.

2. System Modelling: Components and Topology

An LV–HP setup consisting of a PEMFC stack was established in a laboratory. The complete topology with the associated components is presented in Figure 1. The major attributes of the developed PEMFC-based setup are presented in Table 2.

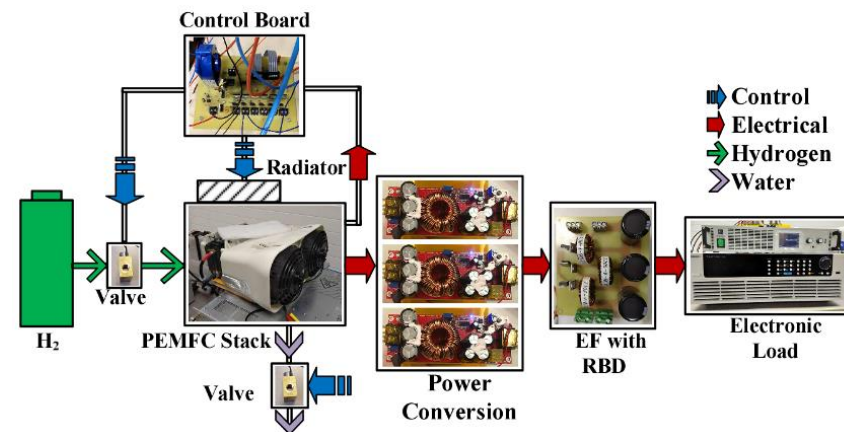


Figure 1. The proposed topology consisting of a PEMFC stack as the main power source.

Table 2. Major attributes of the proposed PEMFC-based setup. (Note: the sign ↓ indicates that the efficiency in general is inferior).

0.7–0.8 V per cell (validated) => Stacking in series for higher voltage	
Variable high current => Capability to drive HP load	
Problem	Proposed solution
Higher losses and poor reliability in power conditioning => Efficiency ↓	Splitting and processing the power through PCCs

The studied topology consists of the following components: (i) a Ballard's 810 W PEMFC stack; (ii) a power-conditioning unit consisting of three BCs coupled in parallel; (iii) an equalization filter combined with reverse blocking diodes (RBDs); and (iv) an electronic programmable load. Numerical simulations are also performed in MATLAB/Simulink using a scaled-up version consisting of a PEMFC (6 kW) and other components from the MATLAB/Simulink built-in libraries. The details and specifications of the components utilized in both the simulations and the experimental setup are presented in Appendix A: Table A1.

2.1. PEMFC as Main Power Source

A PEMFC was given preference owing to its compact size, high power density, low operating temperature, and rapid response time [18,33]. It generally displays a soft behavior that follows nonlinearly decreasing voltages rather than the power drawn from it [24,25]. In a static FC model [37], the non-linear polarization relationship between the voltage and the current of the FC is mathematically defined using Equation (1).

$$V_{fc} = E_0 - V_{act} - V_{ohm} + V_{con} \quad (1)$$

where V_{fc} is the FC stack's voltage and E_0 is the no load voltage (Nernst voltage). E_0 can be calculated using the relation given in Equation (2), which shows that E_0 is dependent on the temperature of stack T_{fc} and the partial pressure of hydrogen P_{H_2} and of oxygen P_{O_2} .

$$E_0 = 1.229 - 0.85 \times 10^{-3} (T_{fc} - 298.15) + 4.3085 \times 10^{-3} T_{fc} \left[\ln(P_{H_2}) + \frac{1}{2} \ln(P_{O_2}) \right] \quad (2)$$

Following Equation (1), besides E_0 , the voltage of the FC (V_{fc}) stack is also dependent on three separate voltage drops, mathematically expressed in Equation (3).

$$\begin{aligned} V_{act} &= A \cdot \log\left(\frac{I_{fc} - i_n}{i_0}\right) \\ V_{ohm} &= R_m (I_{fc} - i_n) \\ V_{con} &= B \cdot \log\left(1 - \frac{I_{fc} - i_n}{i_{lim}}\right) \end{aligned} \quad (3)$$

where I_{fc} is the current delivered by the FC stack, i_0 is the exchange current, A is the slope of the Tafel line, i_{lim} is the limiting current, B is the mass transfer constant, i_n is the internal current, and R_m is the membrane and contact resistance.

In Equation (3), the polarization relation between the FC stack's voltage (V_{fc}) and its current (I_{fc}) is generally divided into three parts: (i) *Activation region*: This occurs at low current density and is mathematically explained using the Tafel equation denoted by V_{act} [37,38]. The voltage in this region decreases exponentially due to the slow chemical reactions that occur at the electrode surface. Depending on the operating temperature and pressure, the type of electrode used, and the catalyst used, this region is more or less wide; (ii) *Ohmic region*: This occurs at intermediate current densities. In this region, the voltage is proportional to the current density, which is denoted by V_{ohm} [37,38]; (iii) *Concentration region*: Due to the high current density demanded from the FC stack, a sharp decrement in voltage is seen in this region. Mass transfer effects dominate in this region due to the limited access of reactant gasses, and the stack's performance therefore decreases significantly. The relationship in this region is governed by V_{con} [37,38]. In context, the polarization curves of both the 18-cell Ballard's 810 W PEMFC stack (experimental) and the 6 kW PEMFC (simulations) are presented in Figure 2a,b.

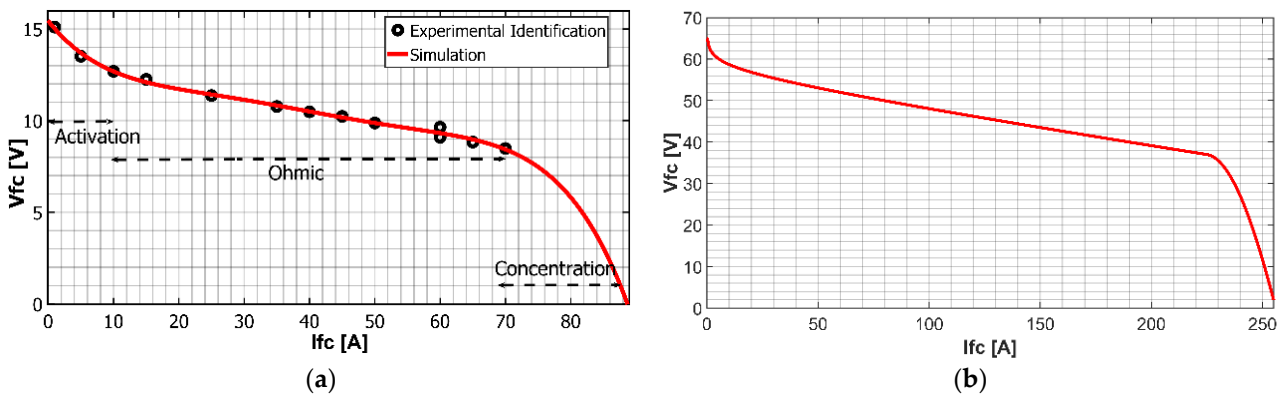


Figure 2. The nonlinear relation between the voltage and current of the PEMFC stack. (a) Polarization curve of 810 W PEMFC stack. (b) Polarization curve of 6 kW PEMFC stack.

2.2. Limitations of CBC

As PEMFCs are LV power sources, a BC is frequently utilized to couple the FC with rest of the system. A generic circuit diagram of the CBC is presented in Figure 3. The operating efficiency and voltage gain of the BC are the two most important performance indicators to consider while regulating the output voltage at a desired value. Regarding efficiency, a major portion of the power losses in BCs are derived from switching phenomena and conduction losses in passive elements [16]. In particular, power losses in passive elements such as the inductor are common when using a CBC for HP processing. Thus, the realization of HP conditions can lead to a reduction in conversion efficiency and voltage gain during the power-processing phase due to excessive power losses.

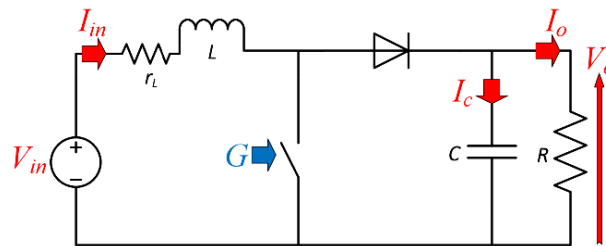


Figure 3. Electrical circuit diagram of the boost converter.

$G \in [0, 1]$ is the switching sequence or duty cycle. An average CBC model for the whole switching period is given in Equation (4) [16].

$$\begin{aligned}
 V_L &= L \frac{dI_{in}}{dt} = V_{in} - I_{in}r_L - (1 - G)V_o \\
 I_c &= C \frac{dV_o}{dt} = (1 - G)I_{in} - \frac{V_o}{R}
 \end{aligned}
 \tag{4}$$

By considering the inductor’s current (I_{in}) and the capacitor’s voltage (V_o) as two active states, the converter model can be modified as follows:

$$\begin{aligned}
 \dot{I}_{in} &= \frac{1}{L}[V_{in} - I_{in}r_L - (1 - G)V_o] \\
 \dot{V}_o &= \frac{1}{C}[(1 - G)I_{in} - \frac{V_o}{R}]
 \end{aligned}
 \tag{5}$$

In a steady state condition, the derivatives of the states are zero. Consequently, Equation (5) is as follows:

$$\begin{aligned}
 \dot{I}_{in} &= \frac{1}{L}[V_{in} - I_{in}r_L - (1 - G)V_o] = 0 \\
 \dot{V}_o &= \frac{1}{C}[(1 - G)I_{in} - \frac{V_o}{R}] = 0
 \end{aligned}
 \tag{6}$$

The relation between voltage gain (K) and admittance gain (Y) can be extracted as follows:

$$\begin{aligned} \frac{V_o}{V_{in}} = K &= \frac{1}{G' \left[1 + \frac{r_L/R}{G'^2} \right]} \\ \frac{I_{in}}{V_{in}} = Y &= \frac{1}{G'^2 R \left[1 + \frac{r_L/R}{G'^2} \right]} \end{aligned} \quad (7)$$

where $G' = 1 - G$. Similarly, current gain (J) can be extracted as follows:

$$\begin{aligned} I_{in} &= \frac{V_o}{G'R} = \frac{I_o}{G'} \\ \frac{I_o}{I_{in}} &= J = G' \end{aligned} \quad (8)$$

The efficiency (η) of the converter, considering the inductive resistance (r_L) of the input side inductor, is calculated using Equation (9).

$$\eta = \frac{P_o}{P_{in}} = \frac{V_o I_o}{V_{in} I_{in}} = \frac{V_o G' I_{in}}{V_{in} I_{in}} = \frac{1}{\left[1 + \frac{r_L/R}{G'^2} \right]} \quad (9)$$

Following Equations (7) and (9), both voltage gain and efficiency are modified when inductive resistance (r_L) is considered. The modified expressions are now dependent both on ratio r_L/R and on G . With these modified relations, and with different load resistance (R) values, the variations in K and η are shown against different values of G in Figure 4.

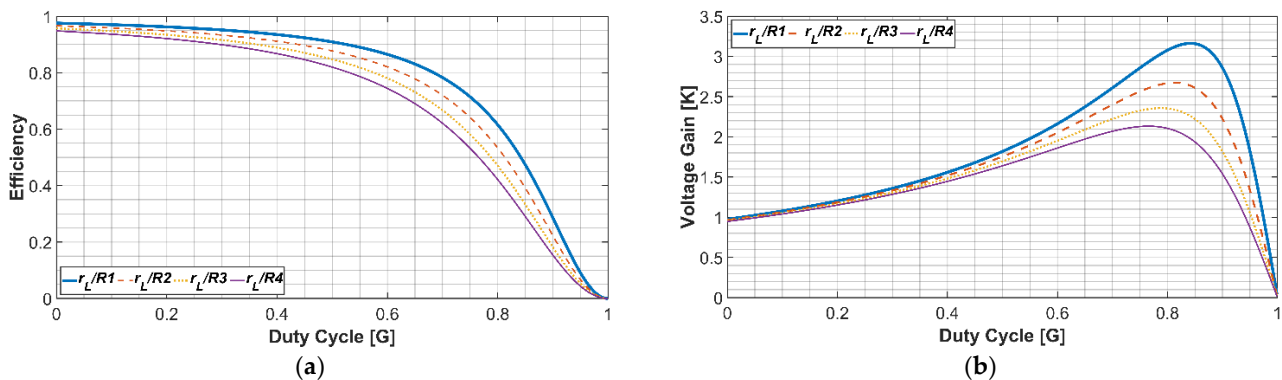


Figure 4. Performance indicators of the practical CBC. (a) Efficiency. (b) Voltage gain.

In Figure 4, a constant r_L value is considered, and load resistance varies according to the relation $R_1 > R_2 > R_3 > R_4$. Reducing the value of R in the ratio r_L/R decreases the voltage gain and the efficiency of the CBC at a specific value of G . Practically, this statement can be attributed to two factors: (i) a higher G value means that the switch is on for a major portion of the switching time, passing current (I_{in}) through r_L , which results in higher losses, poor efficiency, and lower voltage gain; and (ii) the decrease in the R value results in the extraction of more power from the source to meet the higher load current (I_o), therefore decreasing the efficiency. It can also be observed from Equation (7) that regulating the output voltage (V_o) at a desired value with a continuously decreasing source voltage (V_{in}) requires a higher value of G , which results in poor efficiency. In brief, both the efficiency and the voltage gain of the CBC are equally influenced by variable conditions at the load and source sides.

2.3. Equivalent Power Sharing between PCCs

CBCs are limited by lower voltage gain, poor efficiency, higher losses, and higher ripple contents in HP applications. To address these concerns, a unique power-conditioning stage involving PCCs was proposed. The proposed conversion stage has the capability to provide high voltage gain, higher efficiency, and lower ripple contents. The characteristics of the PCCs are vital in HP applications as they must match the soft behavior of the PEMFC

stack. The applications of PCCs are very diverse, e.g., the power-conditioning units in fuel cell hybrid electric vehicles (FCHEVs) [39–41]. In LV–HP applications, instead of processing power through a CBC, a practical solution is to equally split the load power between the PCCs [29,30]. The purpose of splitting the power between the PCCs is to process small shares of the load power through individual converters, resulting in less stress on the components and a decrease in the power losses. The reduction in power losses results in improved electrical efficiency, and the reliability and lifespan of the components are thereby enhanced. Splitting the current also yields lower inductance sizes which reduces the cost, size, heat dissipation, and losses. The performance-limiting constraints associated with PCCs considered in this paper are as follows:

- An unwanted mismatch between the outputs of the coupled converters, leading to an unequal distribution of load power.
- The presence of inner circulating currents due to mismatched outputs. These circulating currents pose a serious threat to the safety of the converters and further deteriorate their power-sharing capability.
- Frequent deviations from the voltage requirement (V_r) at the load side due to unbalanced power sharing and the presence of circulating currents.

Rather than the flexible control structures often proposed in the literature [21,22,34–36] for addressing the aforementioned PCC-related problems, this paper proposes a mixture of decentralized dual-loop controllers and physical compensation. The proposed topology is illustrated in Figure 5 and is as follows:

- A complete control structure (CCS) is formulated consisting of decentralized dual-loop controllers for the tight regulation of output, as is illustrated in Figure 6. Without needing a common communication block, the decentralized controllers work independently for each coupled converter to produce regulated output, thus minimizing the problem of the unbalanced sharing of load power.
- To protect the interconnected converters against inner circulating currents, a network of reverse blocking diodes is provided after the PCCs, as is shown in Figure 5.
- An equalization filter is designed and properly placed between PCCs and the HP load for facilitating both the equivalent sharing of load power and the regulation of the output voltage, even in the presence of a slight offset between the output of the coupled converters.

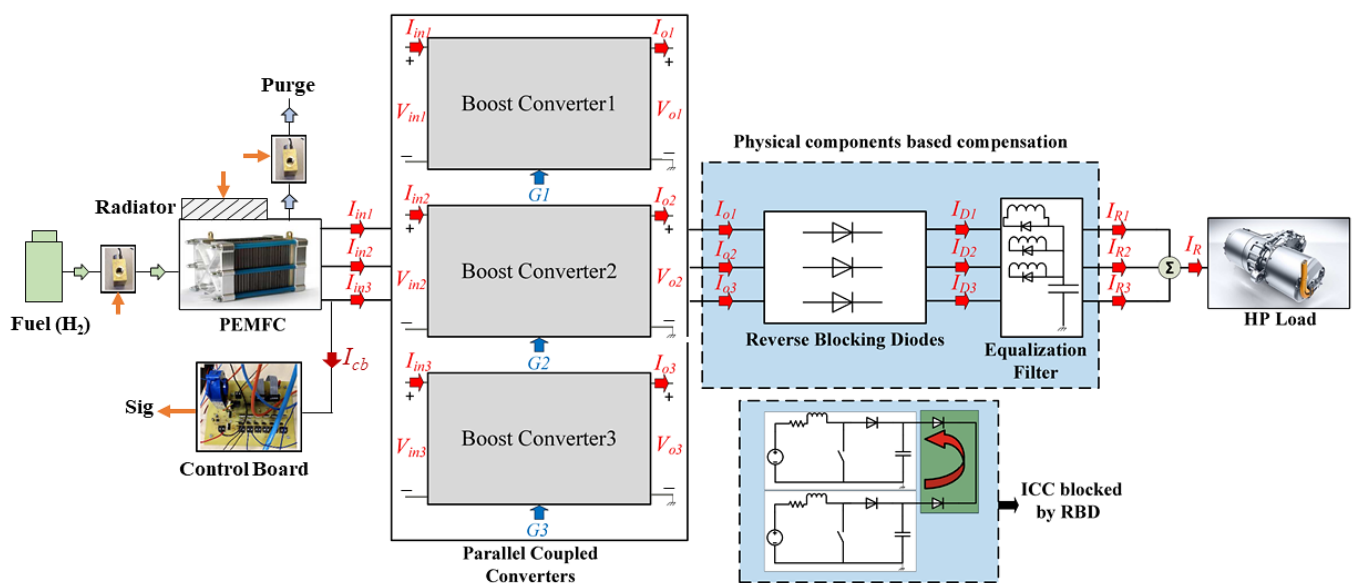


Figure 5. Complete topology of proposed power-sharing strategy.

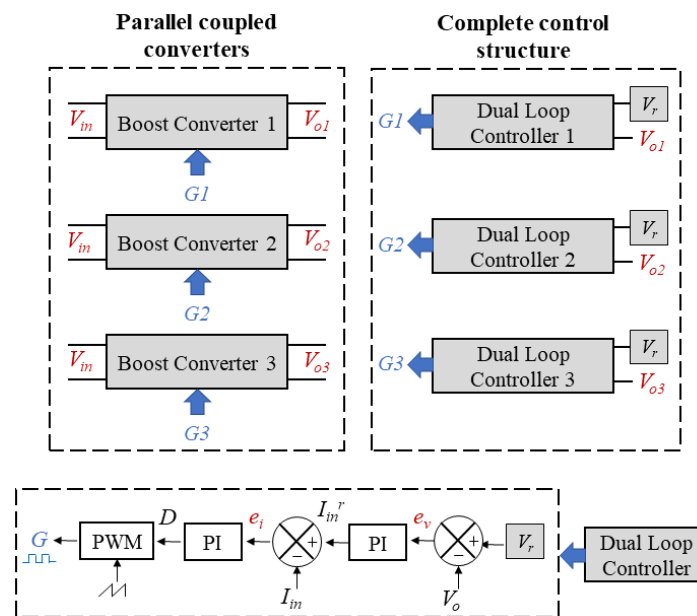


Figure 6. Complete control structure consisting of dual-loop controllers.

3. Numerical Simulations and Discussion

The numerical assessment was performed in a MATLAB/Simulink environment for validating the viability of power sharing between the proposed PCCs under various loading conditions and a wide spectrum of PEMFC voltages (soft behavior). The studied system consists of a PEMFC stack (6 kW) as main power source. The 6 kW PEMFC stack is coupled to an electrical load via three boost converters (connected in parallel). The load profile (uneven incremental/decremental slopes) was designed according to the nominal rating of the PEMFC stack and the electrical demand that could be expected from an automotive application while keeping the DC bus regulated at 75 V. The specifications for the remaining components are given in Appendix A: Table A1. The components were connected together to form the topology illustrated in Figure 5.

Further, the dual-loop complete control structure (CCS) is presented in Figure 6. This structure is very commonly used among researchers [42,43] and is considered a well-established approach. Compared with recent and advance nonlinear controllers (which generally perform better) [44,45], the utilized CCS does not require a mathematical understanding of the model and is easier to implement. The CCS also provides reliable performance, subject to how well the gains of the PI controllers are tuned and how well the overall closed loop is designed. Another feature is that both output voltage regulation (V_r) and input-side current tracking (I_{in}^r) are a simultaneous functionality of the CCS, thus facilitating equivalent sharing among the parallel converters. In this work, the gains were tuned using the heuristic knowledge of the authors, and the performance was found to be satisfactory under a range of tested operating conditions. However, the gains may require retuning if the operational environment changes significantly, highlighting the shortcomings of PI controllers.

Several performance criteria, such as PEMFC voltage (V_{fc}) and current (I_{fc}), electrical efficiency (η), regulation of the output voltage (V_o), and ripples in the output (ΔV_o), were graphically compared for the studied power-conditioning stages. A comprehensive analysis of the results was performed to highlight the benefits and drawbacks of the proposed PCC structure compared with those of a CBC. The simulated and analyzed case study consisted of a randomly changing load with unequal incremental and decremental slopes.

Figure 7 presents a graphical comparison between a CBC power stage and the proposed PCC stage. The corresponding current profiles are displayed in Figure 7a. A small portion with the highest variation in load (highlighted with a star) was selected to provide a comparison between the studied power stages. The attributes which were effectively

compared are the electrical conversion efficiency of the system (Figure 7e), the regulation of the output voltage V_o at desired value $V_r = 75$ V (Figure 7c), the ripples in the output ΔV_o (Figure 7c), and the PEMFC profile, including its current (Figure 7b) and voltage (Figure 7d).

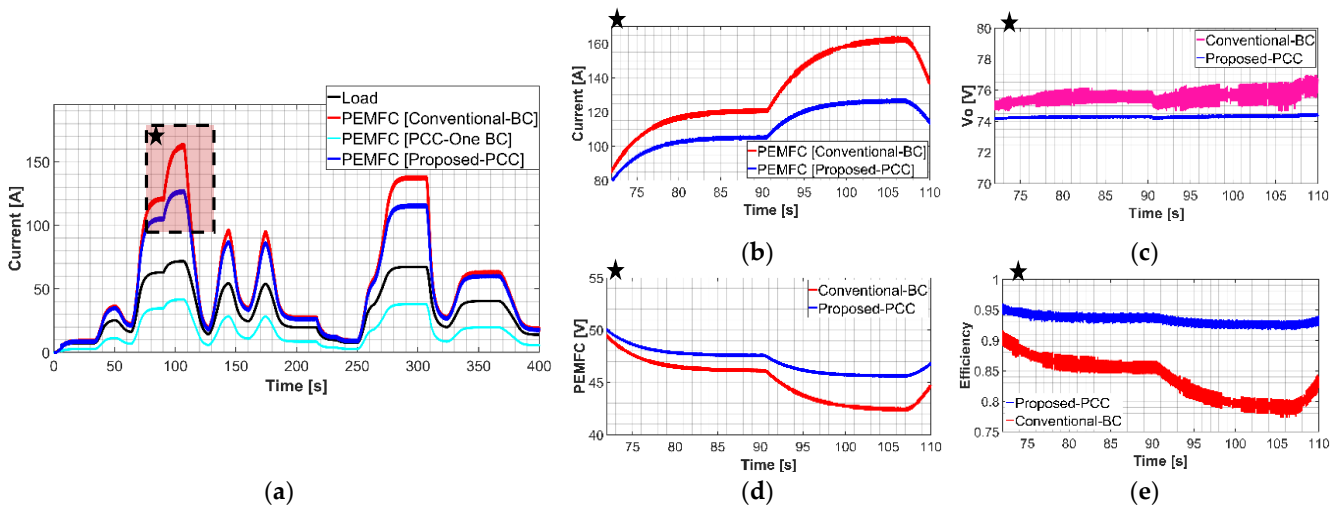


Figure 7. Case study for numerical simulations. (a) Profile and selected area under observation. (b) PEMFC current. (c) Load voltage. (d) PEMFC voltage. (e) Electrical efficiency. Note: A small portion with the highest variation in load (highlighted with a star) denotes the key area of interest.

As Figure 7b,e illustrate, within the selected region, the PEMFC current in the proposed PCCs is up to 25% lower than that of the CBC, which results in a 17% higher conversion efficiency in similar operating conditions. The proposed PCCs also regulate the output V_o at the desired value with reduced ripple contents compared with the CBC (Figure 7c), which indirectly reduces stress and enhances reliability. Mathematically, to regulate the output V_o at the lower PEMFC voltage value of the CBC (Figure 7d), a higher value of G is required, resulting in a higher PEMFC current (Figure 7b). The higher current value increases the power losses (P_l) and consequently reduces the conversion efficiency (Figure 7e). The drastic increase in efficiency is linked to an equivalent power distribution, significantly reducing stress from conversion stage and reducing power losses.

In Figure 8, an overall summary of the simulation results is presented. The load power is equally shared and conditioned by three coupled BCs. The efficiency of the proposed PCCs is significantly higher, particularly at higher load currents. When the load current is 72 A, the proposed PCCs provide an approximately 18% higher conversion efficiency and lower losses compared with those of the CBC.

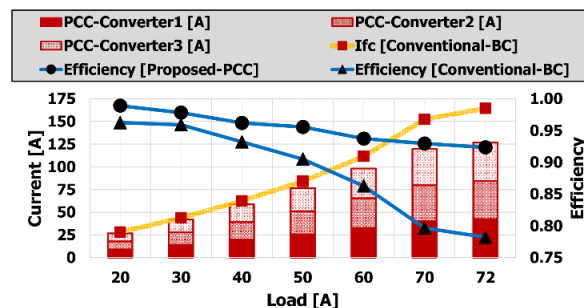


Figure 8. Overall summary of simulation results.

As Figures 7 and 8 show, it is evident from the simulation environments that if the performance-limiting constraints affecting the PCC, such as inner circulating currents, the tight regulation of output voltages, and the equal sharing of the current, are properly addressed; a significantly efficient power-conversion stage can be achieved, particularly favorable for fuel cell-based high-power applications.

4. Experimental Setup: Results and Discussion

A scaled-down experimental setup was established to validate the practical feasibility of the power-splitting strategy between the proposed PCCs under variable loading conditions. A PEMFC stack (18 cells, 810 W) was used as the main power source. An electronic load was connected to the PEMFC stack via the proposed PCCs and an equalization filter. Table A1 (Appendix A) can be consulted to check the list of components and their individual specifications. The experimental setup is shown in Figure 9. Unlike the numerical simulations, the objective here was to regulate the output (V_o) at $45\text{ V} \pm 5\%$ while the load (I_o) incrementally varied from 1 A to 9 A.

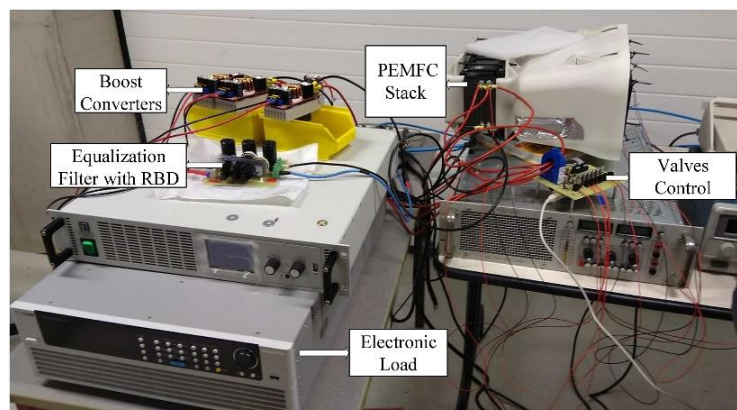


Figure 9. Experimental setup for proposed equivalent power-sharing strategy.

The steps being followed throughout experimental validation were as follows:

Step-1: The parallel-connected BCs were tuned individually to provide a regulated $45\text{ V} \pm 5\%$ at the output (V_o). The equalization filter (EF) was appropriately placed after the converters. The PEMFC stack (the fundamental power source) and the electronic load were connected to the power stage. The connection diagram shown in Figure 5 was followed to complete the connections.

Step-2: Variable loading conditions were practically emulated using an electronic load, and the equivalent sharing of the load power between the converters was examined. In the case of any discrepancy, protection against ICCs was provided using RBDs. These discrepancies were further remedied using an on-board decentralized controller.

Step-3: The effectiveness of the EF in assisting the equivalent power sharing and regulation of the V_o at the desired value was studied and recorded. The main parameters of the PEMFC stack, such as V_{fc} , I_{fc} , and P_{fc} , were carefully recorded. It was ensured that the control board provided adequate control signals to the radiator of the FC and to the electronic valves that regulate the power output of the PEMFC stack.

Step-4: The performance of the proposed PCCs is presented and analyzed in Figure 10. The feasibility of the power-splitting strategy to offload stress from individual converters and increase conversion efficiency under HP conditions was validated.

Note: It was observed that the practical performance of the PCCs was very sensitive to the difference between the outputs of the connected converters and could be bottlenecked by the inappropriate placement of the EF. Furthermore, the presence of the RBDs enhanced the protection required for the reliable operation of the PCCs.

As Figure 10 shows, the processing of HP through the proposed PCC invoked higher current from the PEMFC (I_{fc}), a trend revealed in Figure 10b. In the particular case of higher load power (P_o)@ $I_o = 9\text{ A}$, the current extracted from the PEMFC (I_{fc}) was in the vicinity of 40 A, which is relatively large, and, if processed through a CBC, would significantly reduce the efficiency and consequently the service life of the components. Since the load power was shared by three interconnected converters, reasonably efficient operation was obtained, even when significant load power was processed at a lower PEMFC voltage V_{fc} , as is shown in Figure 10a,b.

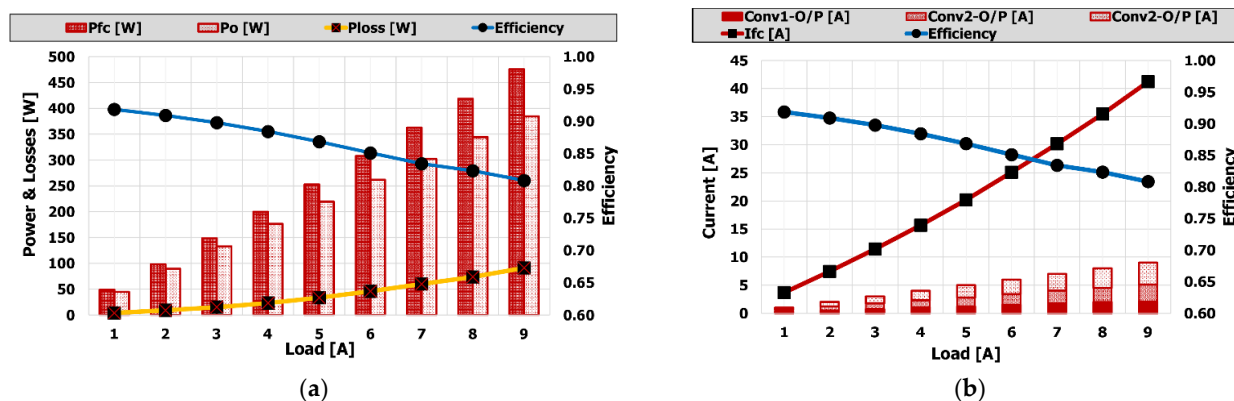


Figure 10. Real-time operation of proposed PCCs in PEMFC-based HP applications. (a) Losses and efficiency. (b) Current sharing and efficiency.

A one-to-one comparison of the efficiency of the proposed PCCs during the simulations (Figure 8) and the experimental validation (Figure 10) indicates that the efficiency of physical model was generally lower than that recorded in the simulations. This can be attributed to the presence of various losses in the real system which were not considered in the simulations. However, the overall trend was the same in both the simulations and the experimental studies, as the results are in consistent agreement for both the simulations and the experimental validation. Accordingly, the distribution of a substantial amount of power through multiple converters, particularly under low-voltage conditions, if properly managed, can increase efficiency and reliability considerably. The converters would thus be subjected to less electrical stress, which would reduce thermal throttling and extend the lifespan of the components.

5. Conclusions and Perspectives

This paper has proposed an efficient physical components-assisted equivalent power distribution strategy between parallel-coupled boost converters. To achieve a balanced sharing of power between the interconnected converters and to enhance operational safety, an equalization filter was provided in conjunction with reverse blocking diodes. The proposed topology is particularly suitable for applications with high power loads. For example, traction motors derived from low-voltage sources, such as FC-based energy systems. The feasibility of the proposed power-sharing strategy was initially assessed using simulation environments developed in MATLAB/Simulink. The simulations revealed that with the proposed strategy, an elevated operational efficiency of approximately 16% is achieved under high-power operating conditions compared with a conventional boost converter. The performance of the proposed stage was also experimentally validated using a setup consisting of a programmable load, an 810 W PEMFC stack, three boost converters, and an equalization filter. Several real-time scenarios were imitated by manipulating programmable devices, and the findings were critically analyzed under varying operating conditions. A consistent agreement was observed between the experimental validations and the simulations under variable operating conditions.

Our main remarks and recommendations concerning the proposed configuration are as follows: (i) the appropriate functioning of the proposed strategy is dependent on the tight matching of the converter's duty cycles; (ii) the precise placement of the equalization filter is necessary for facilitating the equivalent sharing of the load power between the parallel-coupled converters; (iii) the reverse blocking diodes play an important role in enhancing the protection against inner circulating currents; and (iv) the closed-loop regulation combined with minor manual tuning ensures that the converters continue to operate in close proximity and meet the steady voltage requirements. The results obtained through the simulations and the experimental setup clearly demonstrate the reliable and efficient operation of the

parallel-coupled converters under high power loads using the proposed power-sharing strategy and filter topology.

Author Contributions: Validation, A.B.; Investigation, F.C.; Writing—original draft, M.I.; Supervision, M.B. All authors have contributed equally. All authors have read and agreed to the published version of the manuscript.

Funding: This research received no external funding.

Data Availability Statement: Data can be provided on reasonable request.

Conflicts of Interest: The authors declare no conflict of interest.

Nomenclature

Abbreviations

BC	Boost converter
CBC	Conventional boost converter
CSS	Complete control structure
EF	Equalization filter
FC	Fuel cell
FCHEV	Fuel cell hybrid electric vehicle
HP	High power
ICC	Inner circulating currents
IBC	Interleave boost converter
LV	Low voltage
PCC	Parallel-coupled boost converters
PEF	Passive equalization filter
PEMFC	Proton exchange membrane fuel cell
PV	Photovoltaic
RBD	Reverse blocking diodes

Notations

$[V_{fc}, I_{fc}, P_{fc}]$	PEMFC parameters
$[V_{in}, I_{in}, P_{in}]$	Source parameters (in: input)
$[V_o, I_o, P_o, R]$	Load parameters (o: output)
$[K, J, Y]$	Voltage, current, and admittance gains
G	Duty cycle
η	Conversion efficiency
r_L	Inductive resistance
P_{rL}	Power loss
V_L	Inductor voltage
V_r	Voltage reference
I_c	Capacitor current

Appendix A

Table A1. Specifications of the components.

Component		Experimental Setup	Simulations
Source		PEMFC stack (18 cells, 810 W)	PEMFC stack (6 kW)
Load		Electronic load (4 kW)	Controlled current source
EF	FWD	RHRP 3060D	0.8 V-drop model
	L	2700 μ H	20 μ H
	C	4700 μ F	250 μ F
RBD		RHRP 3060D	0.8 V-drop model
BC	r_L		0.05 Ω
	L	1800 W, 40 A	1000 μ H
	C		2200 μ F

References

1. Mounica, V.; Obulesu, Y.P. Hybrid power management strategy with fuel cell, battery, and supercapacitor for fuel economy in hybrid electric vehicle application. *Energies* **2022**, *15*, 4185. [[CrossRef](#)]
2. Iqbal, M.; Becherif, M.; Ramadan, H.S.; Badji, A. Dual-layer approach for systematic sizing and online energy management of fuel cell hybrid vehicles. *Appl. Energy* **2021**, *300*, 117345. [[CrossRef](#)]
3. Felseghi, R.-A.; Carcadea, E.; Raboaca, M.S.; Trufin, C.N.; Filote, C. Hydrogen Fuel Cell Technology for the Sustainable Future of Stationary Applications. *Energies* **2019**, *12*, 4593. [[CrossRef](#)]
4. Mehrjerdi, H.; Iqbal, A.; Rakhshani, E.; Torres, J.R. Daily-seasonal operation in net-zero energy building powered by hybrid renewable energies and hydrogen storage systems. *Energy Convers. Manag.* **2019**, *201*, 112156. [[CrossRef](#)]
5. Zheng, Y.; He, F.; Shen, X.; Jiang, X. Energy Control Strategy of Fuel Cell Hybrid Electric Vehicle Based on Working Conditions Identification by Least Square Support Vector Machine. *Energies* **2020**, *13*, 426. [[CrossRef](#)]
6. Chen, X.; Hu, G.; Guo, F.; Ye, M.; Huang, J. Switched Energy Management Strategy for Fuel Cell Hybrid Vehicle Based on Switch Network. *Energies* **2020**, *13*, 247. [[CrossRef](#)]
7. Duc, T.N.; Goshome, K.; Endo, N.; Maeda, T. Optimization strategy for high efficiency 20 kW-class direct coupled photovoltaic-electrolyzer system based on experiment data. *Int. J. Hydrogen Energy* **2019**, *44*, 26741–26752.
8. Cecilia, A.; Carroquino, J.; Roda, V.; Costa-Castelló, R.; Barreras, F. Optimal Energy Management in a Standalone Microgrid, with Photovoltaic Generation, Short-Term Storage, and Hydrogen Production. *Energies* **2020**, *13*, 1454. [[CrossRef](#)]
9. Liu, H.; Song, Q.; Zhang, C.; Chen, J.; Deng, B.; Li, J. Development of bi-directional DC/DC converter for fuel cell hybrid vehicle. *J. Renew. Sustain. Energy* **2019**, *11*, 44303. [[CrossRef](#)]
10. Jung, S.-K.; Cha, W.-S.; Park, Y.-I.; Kim, S.-H.; Choi, J. Conceptual Design Development of a Fuel-Reforming System for Fuel Cells in Underwater Vehicles. *Energies* **2020**, *13*, 2000. [[CrossRef](#)]
11. Chen, J.; Wang, C.; Li, J.; Jiang, C.; Duan, C. An Input-Parallel-Output-Series Multilevel Boost Converter With a Uniform Voltage-Balance Control Strategy. *IEEE J. Emerg. Sel. Top. Power Electron.* **2019**, *7*, 2147–2157. [[CrossRef](#)]
12. Singh, S.; Chauhan, P.; Aftab, M.A.; Ali, I.; Hussain, S.M.S.; Ustun, T.S. Cost Optimization of a Stand-Alone Hybrid Energy System with Fuel Cell and PV. *Energies* **2020**, *13*, 1295. [[CrossRef](#)]
13. Iqbal, M.; Benmouna, A.; Becherif, M.; Mekhilef, S. Survey on Battery Technologies and Modeling Methods for Electric Vehicles. *Batteries* **2023**, *9*, 185. [[CrossRef](#)]
14. Liu, S.; Gao, Y.; Yang, L. Research on Application of Non-Isolated Three-Port Switching Boost Converter in Photovoltaic Power Generation System. *Electronics* **2019**, *8*, 746. [[CrossRef](#)]
15. Wang, Y.; Ren, X.; Zhang, Z.; Chen, Q. Research on current sharing strategy of parallel LLC resonant converter. In Proceedings of the 2019 IEEE Applied Power Electronics Conference and Exposition (APEC), Anaheim, CA, USA, 17–21 March 2019; pp. 2294–2299.
16. Erickson, R.W.; Maksimovic, D. *Fundamentals of Power Electronics*; Springer Science & Business Media: New York, NY, USA, 2007.
17. Peyghami, S.; Davari, P.; Blaabjerg, F. System-level lifetime-oriented power sharing control of paralleled DC/DC converters. In Proceedings of the 2018 IEEE Applied Power Electronics Conference and Exposition (APEC), San Antonio, TX, USA, 4–8 March 2018; pp. 1890–1895.
18. Zhan, Y.; Guo, Y.; Zhu, J.; Liang, B.; Yang, B. Comprehensive influences measurement and analysis of power converter low frequency current ripple on PEM fuel cell. *Int. J. Hydrogen Energy* **2019**, *44*, 31352–31359. [[CrossRef](#)]
19. Sha, D.; Xu, Y.; Zhang, J.; Yan, Y. Current-Fed Hybrid Dual Active Bridge DC–DC Converter for a Fuel Cell Power Conditioning System With Reduced Input Current Ripple. *IEEE Trans. Ind. Electron.* **2017**, *64*, 6628–6638. [[CrossRef](#)]
20. Cheng, P.; Ding, G.; Song, C.; Chai, H.; Xu, G. Stability Analysis of Identical Paralleled DC-DC Converters with Average Current Sharing. In Proceedings of the 2019 IEEE Asia Power and Energy Engineering Conference (APEEC), Chengdu, China, 29–31 March 2019; pp. 60–64.
21. Xia, Y.; Wei, W.; Peng, Y.; Yang, P.; Yu, M. Decentralized Coordination Control for Parallel Bidirectional Power Converters in a Grid-Connected DC Microgrid. *IEEE Trans. Smart Grid* **2018**, *9*, 6850–6861. [[CrossRef](#)]
22. Wang, H.; Han, M.; Han, R.; Guerrero, J.M.; Vasquez, J.C. A Decentralized Current-Sharing Controller Endows Fast Transient Response to Parallel DC–DC Converters. *IEEE Trans. Power Electron.* **2018**, *33*, 4362–4372. [[CrossRef](#)]
23. Yang, P.; Xia, Y.; Yu, M.; Wei, W.; Peng, Y. A Decentralized Coordination Control Method for Parallel Bidirectional Power Converters in a Hybrid AC–DC Microgrid. *IEEE Trans. Ind. Electron.* **2018**, *65*, 6217–6228. [[CrossRef](#)]
24. Wang, P.; Zhou, L.; Zhang, Y.; Li, J.; Sumner, M. Input-Parallel Output-Series DC-DC Boost Converter with a Wide Input Voltage Range, for Fuel Cell Vehicles. *IEEE Trans. Veh. Technol.* **2017**, *66*, 7771–7781. [[CrossRef](#)]
25. Zúñiga-Ventura, Y.A.; Langarica-Córdoba, D.; Leyva-Ramos, J.; Díaz-Saldierna, L.H.; Ramírez-Rivera, V.M. Adaptive Backstepping Control for a Fuel Cell/Boost Converter System. *IEEE J. Emerg. Sel. Top. Power Electron.* **2018**, *6*, 686–695. [[CrossRef](#)]
26. Garrigós, A.; Marroquí, D.; García, A.; Blanes, J.M.; Gutiérrez, R. Interleaved, switched-inductor, multi-phase, multi-device DC/DC boost converter for non-isolated and high conversion ratio fuel cell applications. *Int. J. Hydrogen Energy* **2019**, *44*, 12783–12792. [[CrossRef](#)]
27. Wu, J.; Lu, Y. Adaptive Backstepping Sliding Mode Control for Boost Converter With Constant Power Load. *IEEE Access* **2019**, *7*, 50797–50807. [[CrossRef](#)]

28. Gao, D.; Jin, Z.; Liu, J.; Ouyang, M. An interleaved step-up/step-down converter for fuel cell vehicle applications. *Int. J. Hydrogen Energy* **2016**, *41*, 22422–22432. [[CrossRef](#)]
29. Sha, D.; Xu, G. Dynamic Response Improvements of Parallel-Connected Bidirectional DC–DC Converters. In *High-Frequency Isolated Bidirectional Dual Active Bridge DC–DC Converters with Wide Voltage Gain*; Springer: Singapore, 2019; pp. 279–303.
30. Ruan, X.; Chen, W.; Fang, T.; Zhuang, K.; Zhang, T.; Yan, H. A General Control Strategy for DC–DC Series–Parallel Power Conversion Systems. In *Control of Series-Parallel Conversion Systems*; Springer: Singapore, 2019; pp. 29–53.
31. Al-Saud, M.S. Interleaved boost converter for global maximum power extraction from the photovoltaic system under partial shading. *IET Renew. Power Gener.* **2019**, *13*, 1232–1238.
32. Peng, D.; Huang, M.; Li, J.; Sun, J.; Zha, X.; Wang, C. Large-Signal Stability Criterion for Parallel-Connected DC–DC Converters With Current Source Equivalence. *IEEE Trans. Circuits Syst. II Express Briefs* **2019**, *66*, 2037–2041. [[CrossRef](#)]
33. Slah, F.; Mansour, A.; Hajer, M.; Faouzi, B. Analysis, modeling and implementation of an interleaved boost DC-DC converter for fuel cell used in electric vehicle. *Int. J. Hydrogen Energy* **2017**, *42*, 28852–28864. [[CrossRef](#)]
34. Luis, F. Master–slave DC droop control for paralleling auxiliary DC/DC converters in electric bus applications. *IET Power Electron.* **2017**, *10*, 1156–1164.
35. Son, Y.; Chee, S.; Lee, Y.; Sul, S.; Lim, C.; Huh, S.; Oh, J. Suppression of Circulating Current in parallel operation of three-level converters. In Proceedings of the 2016 IEEE Applied Power Electronics Conference and Exposition (APEC), Long Beach, CA, USA, 20–24 March 2016; pp. 2370–2375.
36. Iqbal, M.; Benmouna, A.; Eltoumi, F.; Claude, F.; Becherif, M.; Ramadan, H.S. Cooperative Operation of Parallel Connected Boost Converters for Low Voltage-High Power Applications: An Experimental Approach. *Energy Procedia* **2019**, *162*, 349–358. [[CrossRef](#)]
37. Larminie, J.; Dicks, A.; McDonald, M.S. *Fuel Cell Systems Explained*; Wiley: Chichester, UK, 2003.
38. Saadi, A.; Becherif, M.; Aboubou, A.; Ayad, M.Y. Comparison of proton exchange membrane fuel cell static models. *Renew. Energy* **2013**, *56*, 64–71. [[CrossRef](#)]
39. Iqbal, M.; Laurent, J.; Benmouna, A.; Becherif, M.; Ramadan, H.S.; Claude, F. Ageing-aware load following control for composite-cost optimal energy management of fuel cell hybrid electric vehicle. *Energy* **2022**, *254*, 124233. [[CrossRef](#)]
40. Ahmadi, S.; Bathaee, S.M.T. Multi-objective genetic optimization of the fuel cell hybrid vehicle supervisory system: Fuzzy logic and operating mode control strategies. *Int. J. Hydrogen Energy* **2015**, *40*, 12512–12521. [[CrossRef](#)]
41. Iqbal, M.; Ramadan, H.S.; Becherif, M. Health-aware frequency separation method for online energy management of fuel cell hybrid vehicle considering efficient urban utilization. *Int. J. Hydrogen Energy* **2021**, *46*, 16030–16047. [[CrossRef](#)]
42. Chen, Z.; Gao, W.; Hu, J.; Ye, X. Closed-loop analysis and cascade control of a nonminimum phase boost converter. *IEEE Trans. Power Electron.* **2010**, *26*, 1237–1252. [[CrossRef](#)]
43. Yanarates, C.; Zhou, Z. Design and cascade PI controller-based robust model reference adaptive control of DC-DC boost converter. *IEEE Access* **2022**, *10*, 44909–44922. [[CrossRef](#)]
44. Jiang, W.; Zhang, X.; Guo, F.; Chen, J.; Wang, P.; Koh, L.H. Large-signal stability of interleave boost converter system with constant power load using sliding-mode control. *IEEE Trans. Ind. Electron.* **2019**, *67*, 9450–9459. [[CrossRef](#)]
45. Zhang, H.; Li, Y.; Li, Y.; Yuan, C.; Liang, B.; Huangfu, Y. Composite Fast Terminal Sliding Mode Control of DC-DC Converters for Renewable Energy Systems. In Proceedings of the 2022 IEEE Industry Applications Society Annual Meeting (IAS), Detroit, MI, USA, 9–14 October 2022; pp. 1–6.

Disclaimer/Publisher’s Note: The statements, opinions and data contained in all publications are solely those of the individual author(s) and contributor(s) and not of MDPI and/or the editor(s). MDPI and/or the editor(s) disclaim responsibility for any injury to people or property resulting from any ideas, methods, instructions or products referred to in the content.